# Electronic Supplementary Information

# High energy density asymmetric all-solid-state supercapacitor based on cobalt carbonate hydroxide nanowire covered N-doped graphene and porous graphene electrodes

**Hao Xie,‡ Shaochun Tang,‡,* Jian Zhu, Sascha Vongehr, Xiangkang Meng***

Institute of Materials Engineering, National Laboratory of Solid State Microstructures, College of Engineering and Applied Sciences, Nanjing University, Nanjing 210093, Jiangsu, People's Republic of China

Fax: (+86)-25-83595535 E-mail: tangsc@nju.edu.cn; mengxk@nju.edu.cn.

**Figure Captions:**

**Fig. S1** (a) Photograph of NG hydrogel from the hydrothermal synthesis. (b) Low- and (c) high-magnification SEM images of porous NG after freeze drying. (d) SEM image of the NG after cutting into thin film and pressing onto Ni foam.

**Fig. S2** (a) XRD patterns of the GO precursor and resulting porous NG, (b) FT-IR spectrum of the optimal CCH-NG composite and the porous NG, (c) XPS survey and (d) high resolution XPS spectrum of *C*1*s* recorded from the CCH-NG composite.

**Fig. S3** SEM images of CCH-NG composites obtained with the lowest and highest $Co^{2+}$ concentrations of (a) 2 mM and (b) 12 mM, which result in CCH contents of 25.1 and 84.5 wt%.

**Fig. S4** CV curves of bare Ni foam (a) and comparison with the optimal CCH-NG composite (b) at a scan rate of 100 mV $s^{-1}$.

**Fig. S5** Ragone plot comparison between optimal CCH-NG composite and pure CCH.

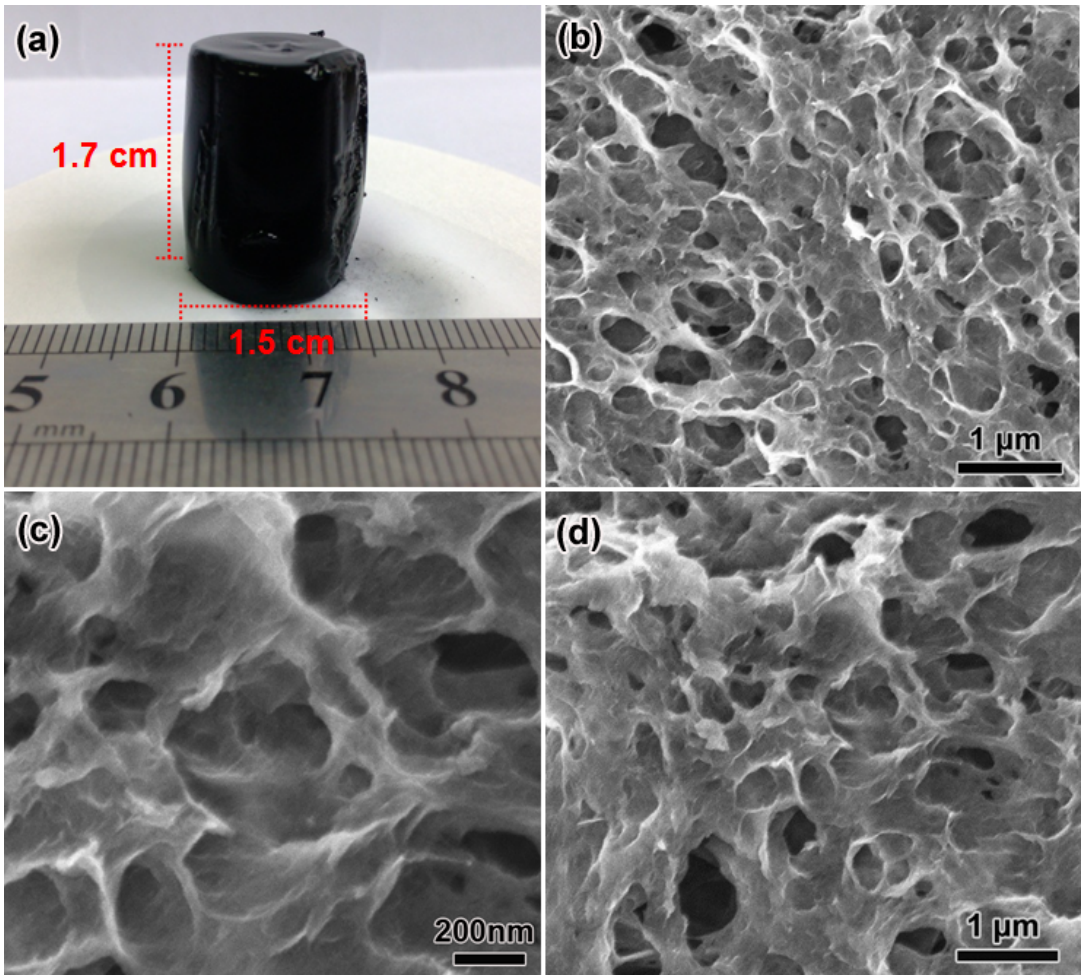


**Fig. S1** (a) Photograph of NG hydrogel from the hydrothermal synthesis. (b) Low- and (c) high-magnification SEM images of porous NG after freeze drying. (d) SEM image of the NG after cutting into thin film and pressing onto Ni foam.

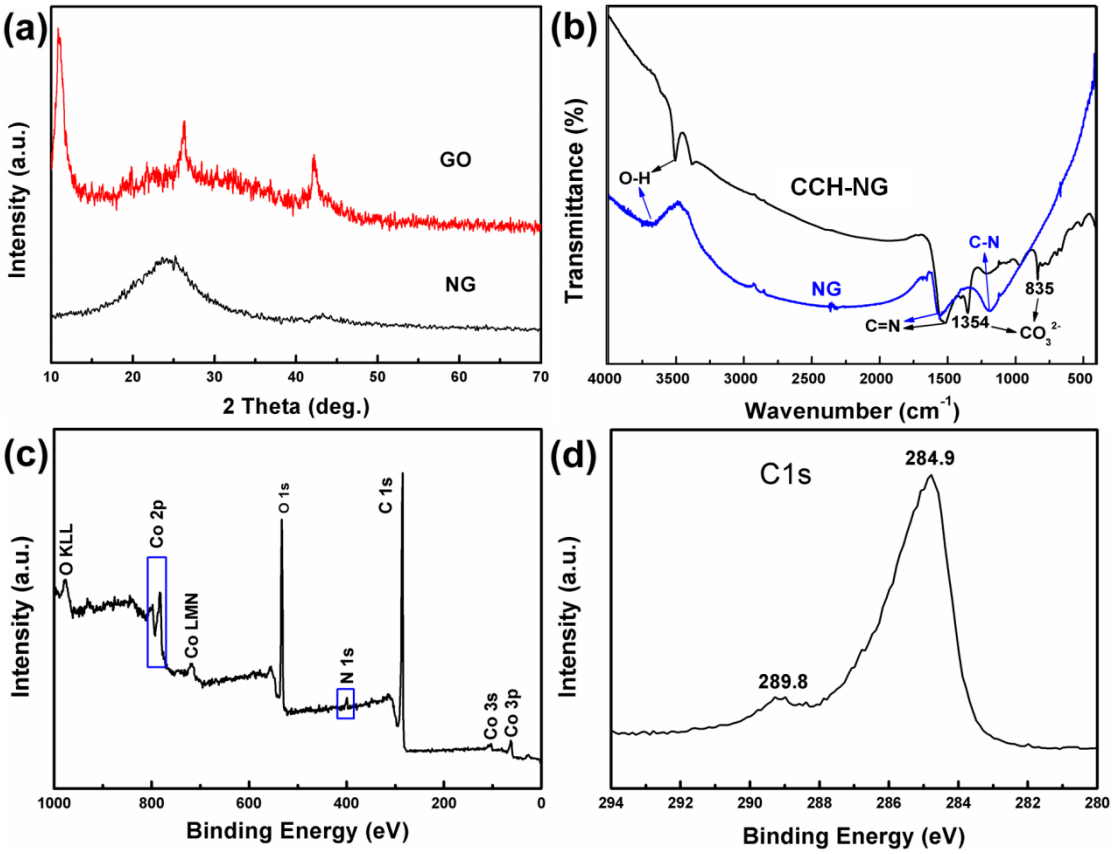


**Fig. S2** (a) XRD patterns of the GO precursor and resulting porous NG, (b) FT-IR spectrum of the optimal CCH-NG composite and the porous NG, (c) XPS survey and (d) high resolution XPS spectrum of *C*1*s* recorded from the CCH-NG composite.

Fig. S2(a) shows XRD patterns of GO (red curve) and resulting NG (black curve). A broad and weak diffraction is observed at about 26.4° and assigned to be the (002) of graphene. The inter-layer spacing is calculated to be 3.42 Å, which is much lower than that of the precursor GO (8.02 Å), but slightly higher than that of natural graphite (3.37 Å). The characteristic GO peak at 11.03° is not visible, indicating the complete conversion to graphene. No peaks from other phases are present. Fig. S2(b) shows FT-IR spectra of the optimal CCH-NG composite and NG. The O-H, C=N, and $CO_3^{2-}$ functional groups are obvious. The little sharp peak at 3510 $cm^{-1}$ is ascribed to the O-H stretching vibration of water molecules and H-bonded OH groups. A notable C=N stretching vibration mode occurs near 1531 $cm^{-1}$, resulting from the NG in the composite. Oxygenated functional groups are almost invisible, indicating a good reduction of GO. The peaks at 1354 $cm^{-1}$, 1217 $cm^{-1}$ and 835 $cm^{-1}$ correspond to the stretching vibrations of $CO_3^{2-}$ in CCH. XPS is often utilized as an effective surface-analyzing technique to investigate the elemental surface composition of samples and the corresponding valence states. The XPS survey of Fig. S2(c) shows anticipated binding energy positions, corresponding to C, O, N and Co elements. The peak of Co2*p* is separated into Co2$p_{3/2}$ and Co2$p_{1/2}$. In the C1s spectrum (Fig. S2(d)), the peak at the binding energy of 289.8 eV is ascribed to *C*1*s* of $CO_3^{2-}$ in CCH.

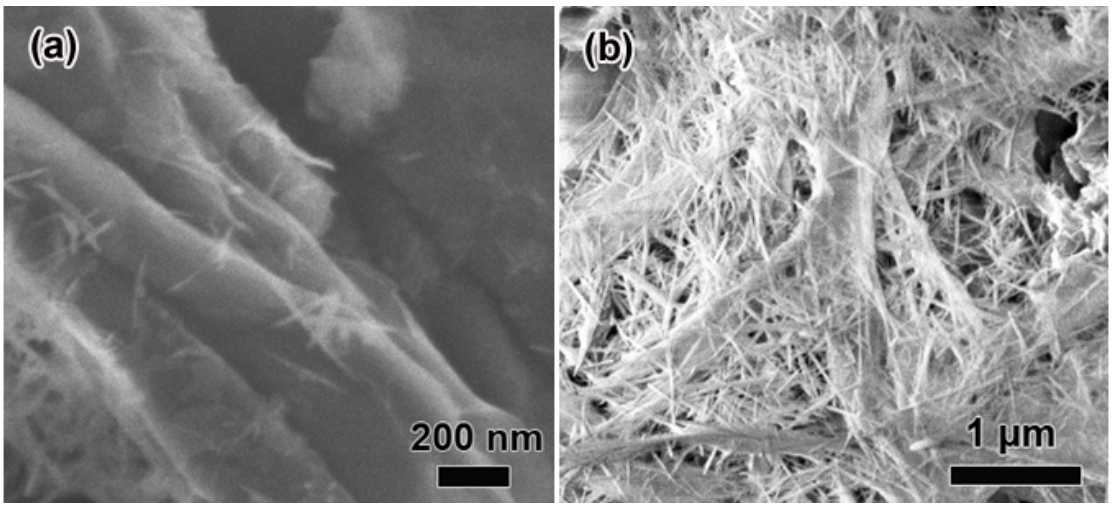


**Fig. S3** SEM images of CCH-NG composites obtained with the lowest and highest $Co^{2+}$ concentrations of (a) 2 mM and (b) 12 mM, which result in CCH contents of 25.1 and 84.5 wt%.

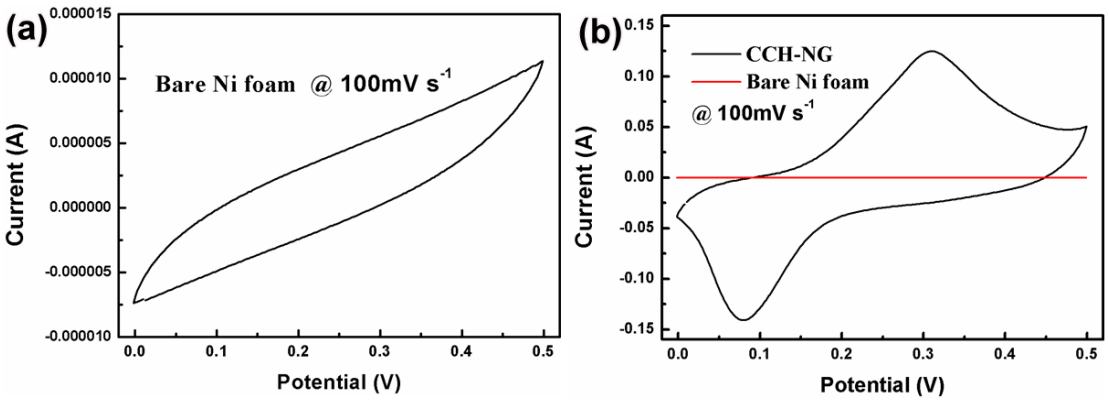


**Fig. S4** CV curves of bare Ni foam (a) and comparison with the optimal CCH-NG composite (b) at a scan rate of 100 mV $s^{-1}$.

Fig. S4(a) shows CV curve of a bare Ni foam measured in 6 M KOH solution. A weak current response is observed, indicating a low capacitance at a high scan rate of 100 mV $s^{-1}$. When comparing with the optimal CCH-NG composite (Fig. S4(b)), this low capacitance derived from bare Ni foam is ignorable. Note that nickel oxide formed on surface of the Ni foam, which contributes to the capacitance, was removed completely via repeated treatments using NaOH, HCl, alcohol and deionized water successively.

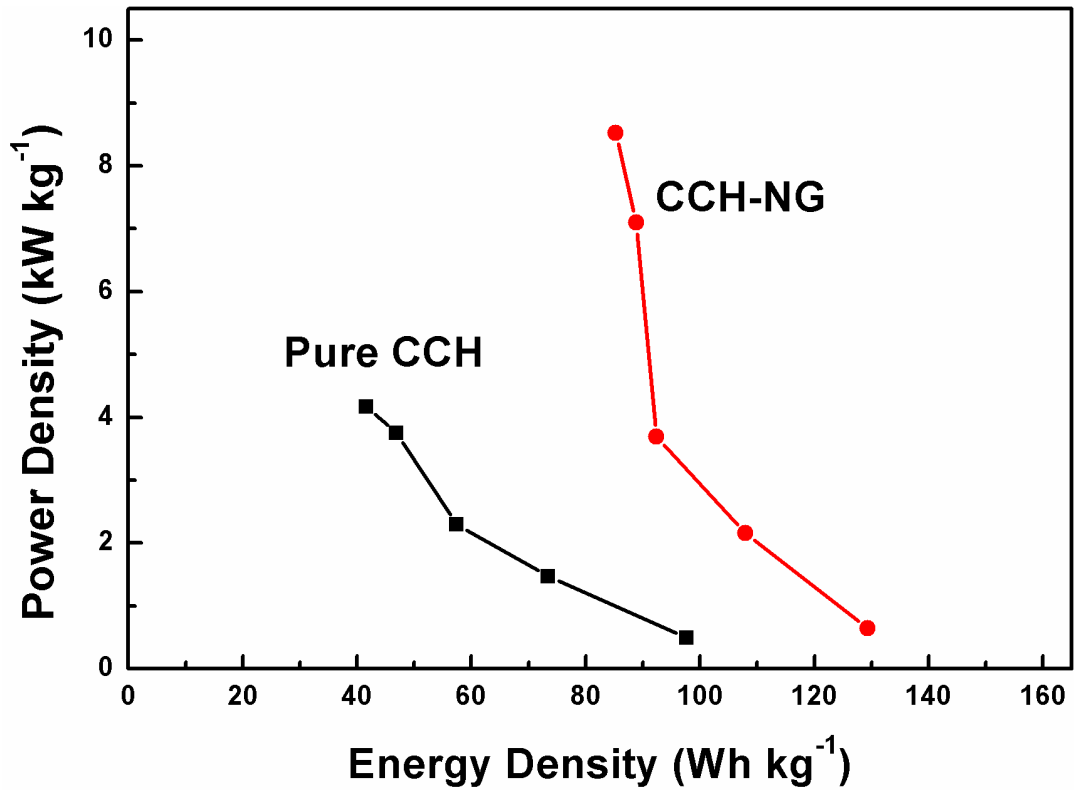


**Fig. S5** Ragone plot comparison between optimal CCH-NG composite and pure CCH.

Energy density of the active materials was derived from the CV curves using $w = C_s(\Delta V)^2/2$, where ΔV is the voltage range of one sweep segment. Power density $w/\Delta t$ derives from $\Delta t$ being the time for one sweep segment. The Ragone plot in Fig. S5 shows that the composite delivers a remarkably high energy density of 85.2 Wh $kg^{-1}$ at a high power density of 8.5 kW $kg^{-1}$, much higher than pure CCH (41.7 Wh $kg^{-1}$ at 4.2 kW $kg^{-1}$).